Nanotechnology **22** (2011) 425701 (6pp) doi:10.1088/0957-4484/22/42/425701

Stable hole doping of graphene for low electrical resistance and high optical transparency

S Tongay[1,2,3], K Berke[1], M Lemaitre[2], Z Nasrollahi[1], D B Tanner[1], A F Hebard[1] and B R Appleton[2]

[1] Department of Physics, University of Florida, Gainesville, FL 32611, USA
[2] Department of Material Science and Engineering, University of Florida, Gainesville, FL 32611, USA

E-mail: tongay@phys.ufl.edu, afh@phys.ufl.edu and appleton@eng.ufl.edu

Received 13 June 2011, in final form 11 August 2011
Published 21 September 2011
Online at stacks.iop.org/Nano/22/425701

Abstract

We report on the p doping of graphene with the polymer TFSA ($(CF_3SO_2)_2NH$). Modification of graphene with TFSA decreases the graphene sheet resistance by 70%. Through such modification, we report sheet resistance values as low as 129 Ω, thus attaining values comparable to those of indium–tin oxide (ITO), while displaying superior environmental stability and preserving electrical properties over extended time scales. Electrical transport measurements reveal that, after doping, the carrier density of holes increases, consistent with the acceptor nature of TFSA, and the mobility decreases due to enhanced short-range scattering. The Drude formula predicts that competition between these two effects yields an overall increase in conductivity. We confirm changes in the carrier density and Fermi level of graphene through changes in the Raman G and 2D peak positions. Doped graphene samples display high transmittance in the visible and near-infrared spectrum, preserving graphene's optical properties without any significant reduction in transparency, and are therefore superior to ITO films in the near infrared. The presented results allow integration of doped graphene sheets into optoelectronics, solar cells, and thermoelectric solar cells as well as engineering of the electrical characteristics of various devices by tuning the Fermi level of graphene.

1. Introduction

Graphene, a single layer of sp^2 bonded carbon atoms, has attracted attention due to its unique physical properties [1] and has been integrated into numerous kinds of devices such as MOSFETs [2], diodes [3, 4], sensors and solar cells [5–7]. In such devices, the electrical characteristics depend on the band misalignment at the graphene/semiconductor–insulator interfaces, and therefore graphene's Fermi level ($E_F^{graphene}$) is an important factor in determining the successful operation of the devices. However, as a result of charge transfer at the graphene/substrate interface, interaction with chemicals used during the transfer process, and contamination/interaction with air, transferred graphene sheets become unintentionally doped. Thus, it is necessary to tune the $E_F^{graphene}$ by controlled doping that is stable for long periods of time without significant changes in graphene's unique optical properties. More recently, graphene electrodes have been used in optoelectric devices/solar cells [6, 8] in an attempt to replace ITO, which is both more expensive and less transparent in the near infrared. Despite graphene's superior optical properties, the conductivity of graphene sheets remains well below commercial ITO films, resulting in reduction of device efficiency.

So far graphene has been p (hole) and n (electron) doped using various methods [9], such as gating [1], chemical [10, 11], and substitutional doping [12, 13]. Electrical gating is undesirable for device applications as it requires application of bias voltages up to 100 V for operation. Chemical and substitutional doping avoid this necessity, but the deposition of atoms, molecules, and polymers onto graphene typically is unstable in atmospheric conditions, resulting in

[3] Author to whom any correspondence should be addressed.

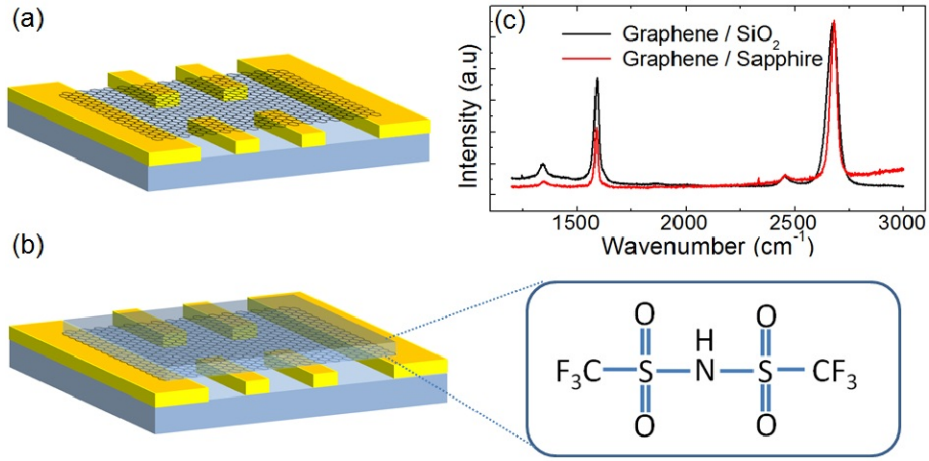

Figure 1. (a) Undoped and (b) doped graphene sheets were transferred onto SiO_2/Si or sapphire substrates and were in contact with Au/Cr contact pads improving electrical contact. Inset, molecular formula of TFSA. (c) Raman spectra taken on graphene transferred onto SiO_2/Si and sapphire substrates.

(This figure is in colour only in the electronic version)

unintentional time dependent electrical properties [1], while substitutional doping induces disorder in the graphene, thereby reducing its mobility [10, 11, 13]. Additionally, most doping processes decrease the optical transparency of devices either by changing the graphene band structure or by forming optically reflective nanoparticles at the surface [14], thus proving detrimental to solar cell/optoelectronic applications where harvesting or emitting light through graphene electrodes is vital.

In this paper, we report on p doping of graphene by modifying the surface with bis(trifluoromethanesulfonyl)amide, TFSA ($[CF_3SO_2]_2NH$). We study electrical and optical properties of TFSA/graphene at temperatures from 300 K down to 5 K and fields from 0 to 7 T. We find that the graphene sheet resistance decreases by 70% while the optical transparency decreases by only 3% after doping. The sheet resistance of graphene initially exhibiting high values has been reduced through doping to values reaching as low as 129 Ω, which is comparable to the resistance of 150–300 Å thick ITO thin films. Electrical properties of TFSA/graphene remain unchanged over time in the atmosphere, displaying superior environmental stability owing to TFSA's hydrophobic character. Electrical transport measurements support increased hole carrier density in graphene after charge transfer. Within the Drude formula, the increase in n_h is accompanied by a slight decrease in mobility μ that results in an overall increase in the conductivity. The effect of TFSA doping on the carrier density of graphene was confirmed by Raman spectroscopy measurements. The increase in the peak position of the G and 2D peaks and a decrease in the 2D to G peak intensity ratio (I_{2D}/I_G) imply that graphene becomes hole doped after interacting with TFSA. The intensity of the D peak remains unchanged after doping, meaning that the doping process does not induce additional defects in the system. Moreover, TFSA doped graphene displays excellent optical transparency in the visible and near-infrared spectrum where ITO and fluorine–tin oxide (FTO) thin films strongly absorb light in the NIR range. Our results demonstrate reproducible modulation of $E_F^{graphene}$, enhanced conductivity with environmental stability and an almost negligible change in the optical transparency of graphene.

2. Experimental details

Large area graphene sheets were synthesized on 25 μm thick copper foils using a multi-step, low pressure chemical vapor deposition (CVD) process [15]. After the graphene growth, 1 μm thick poly(methyl methacrylate) (PMMA) (11% in anisole) was spin-cast on one side of the Cu foils at 2500 rpm for 2 min and post-baked at 125 °C for 3 min, allowing the PMMA to harden. Prior to the Cu etching step, the backsides of the Cu foils were etched in O_2 plasma for 15 s to remove the unwanted graphene. Cu films were then etched in a 0.05 mg l^{-1} solution of $Fe(III)NO_3$ for 12 h to remove the copper foils. The PMMA supported graphene films were then washed in deionized water multiple times to remove contaminants absorbed on the graphene surface during etching and dried using N_2 gas.

Prior to graphene transfer, Au/Cr (50 nm/1 nm) contact pads were evaporated in a six-terminal configuration (figure 1(a)) onto SiO_2/Si substrates by thermal evaporation at 8×10^{-7} Torr pressure. While the gold (Au) pads allow good electrical contact to the graphene sheets, the contact configuration in figure 1 allows us to measure the sheet resistance, Hall voltage, and number of carriers in graphene. Graphene sheets were then transferred onto electrical contact pads, SiO_2, and sapphire substrates by applying a drop of isopropyl alcohol (IPA) onto the substrates and placing PMMA–graphene on top. After the transfer, the PMMA thin films were dissolved in an acetone vapor bath overnight followed by acetone and IPA baths. The transferred graphene sheets were identified/characterized using a Horiba-Yvon micro-Raman spectrometer with a green (532 nm) laser.

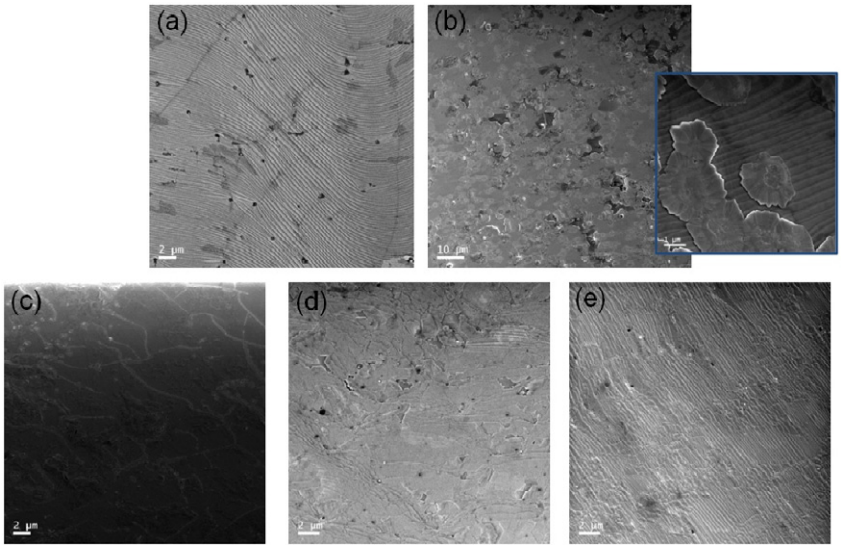

Figure 2. Scanning electron microscope (SEM) images taken on (a) graphene sheets grown onto copper foils and TFSA modified graphene sheets by spin-casting TFSA at (b) 800 rpm, (c) 1100 rpm, (d) 1700 rpm, (e) 2500 rpm. Scales are indicated in each image respectively.

The organic dopant, TFSA, was dissolved in nitromethane (20 mM) and spin-cast onto transferred graphene sheets at 1200–2500 rpm for 1 min. Surfaces were analyzed by scanning electron microscopy (SEM) (figures 2(a)–(d)) and Raman spectroscopy (figure 1(c)). Electrical properties of the pristine and TFSA modified graphene were measured in a six-terminal contact configuration from 300 down to 5 K and from 0 to 7 T magnetic field range. Optical spectra of the quartz, TFSA/quartz, graphene/quartz and TFSA/graphene/quartz were measured in the visible and near-infrared range (figure 5) using a Zeiss microscope photometer with xenon and tungsten lamps as a light source.

3. Results and discussion

Polymers, atoms and gases absorbed on graphene are prone to desorption and therefore chemically doped graphene has previously been found to degrade over time [9]. We avoid degradation of electrical properties by using TFSA; hydrophobic TFSA is an excellent candidate for doping graphene for long term environmental stability. Electrical properties of transferred large area graphene sheets were measured on seven different samples with graphene sheet resistance values (R_{graphene}) ranging from 0.5 to 5.0 kΩ. This wide range of R_{graphene} values can be attributed to slight differences in growth parameters as well as induced defects/disorder during the transfer process. Figure 3(a) illustrates the change in R_{graphene} with respect to time prior to and after surface modification with TFSA. Upon TFSA doping R_{graphene} consistently decreases by $\sim 70 \pm 2\%$ for all the samples measured, achieving a minimum value of 129 Ω in a sample which originally measured 425 Ω before doping. To this end, our preliminary results show that, while the doping time (the total time required to spin TFSA onto the graphene sheets) does not significantly change the doping level, increasing the TFSA concentration up to 20 mM allows one to control (increase) the doping level, and thus the conductivity of the sample. Increasing the TFSA concentration beyond 20 mM no longer affects sample conductivity. The improvement in graphene's sheet conductivity can be attributed to the electron-acceptor nature of TFSA, inducing hole carriers after adhering (figures 2(a)–(d)) to the graphene surface. We note that the $R^{\text{doped}}_{\text{graphene}}$ values depend on the initial value of each graphene sheet's resistance, R_{graphene}, implying that the initial value of graphene's E_{F} as well as density of disorder determines the final value of the sheet resistance. Interestingly, the electrical properties of our doped graphene samples are well preserved with only a minuscule increase ($\sim 2.8 \pm 0.5\%$) in $R^{\text{doped}}_{\text{graphene}}$ after one month exposure to atmosphere.

Even though the decrease in R_{graphene} is mostly attributed to the increase in the carrier density n_{h}, within the Drude formula ($\sigma_{\text{graphene}} = n_{\text{h}} e \mu$), the electrical conductivity of graphene depends on the carrier density and mobility μ. To determine the individual effects of changes in n_{h} and μ on the electrical conductivity of the graphene, we measure carrier density at room temperature before and after doping. Hall resistance (R_{xy}) versus magnetic field data taken before doping (figure 3(c) red squares) imply that transferred samples are doped with hole carrier densities of $n_{\text{h}} \sim 1.9 \times 10^{13}$ cm^{-2}. We note that the initial carrier concentration is higher than the values expected for exfoliated graphene. These values can be attributed to impurities induced at the graphene surface by the chemicals, such as acetone and Fe(III)NO_3, used to etch Cu foils to release the graphene sheets and to transfer them to various substrates such as sapphire and SiO_2/Si. The hole carrier density n_{h} increases by 5.2 times to $n_{\text{h}} \sim 9.9 \times 10^{13}$ cm^{-2} after doping (figure 3(c) blue squares). Using the Drude formula in combination with the factor of 3.3 increase in conductivity (corresponding to the 70% decrease in R), we conclude that the increase in n_{h} is compensated by a decrease in mobility to 63% of the original value. In addition, since the Fermi energy in graphene changes as $E_{\text{F}}(n) = \hbar |v_{\text{F}}| \sqrt{n\pi}$, such increases in n_{h} decrease (increase) the $E^{\text{graphene}}_{\text{F}}$ (W_{graphene},

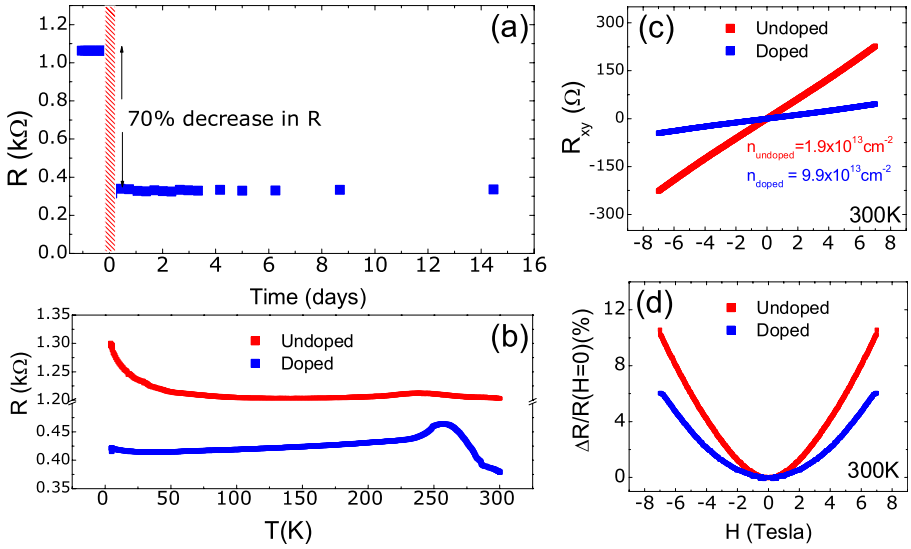

Figure 3. (a) Change in sheet resistance before and after doping with time. The region marked in red indicates when the graphene sheets were doped. (b) Temperature dependence of the graphene sheet resistance before and after doping. (c) Hall resistance (R_{xy}) data and (d) magnetoresistance data taken on doped and undoped graphene sheets at room temperature.

work function of graphene) by ∼0.7 eV due to the acceptor nature of the TFSA polymer.

The mobility of the graphene depends on various factors such as graphene growth parameters, density of disorder [15], number of carriers [16] and coupling of graphene to the substrate. In our measurements, μ was determined from data taken before and after doping with TFSA on the same graphene sheet, thus changes in mobility can only be attributed to doping, independent of variations in the growth parameters used. Moreover, according to Raman spectroscopy measurements, the D peak intensity, associated with the density of disorder in the system, remains unchanged before and after doping, implying that the doping process does not induce additional defects.

So far, a number of scattering processes affecting the carrier mobility in graphene have been proposed and are under active debate. It has been previously reported that graphene's mobility is limited mainly due to the short-range scattering [17], carrier scattering off of the charged impurities [18], and surface optical phonons of SiO_2 (or any dielectric) [19]. Here, charged impurities are assumed to be either on the graphene sheet or at the graphene/substrate interface and they interact with graphene by a Coulomb potential which is inversely proportional to the permittivity of the medium. After transferring graphene onto SiO_2, the average permittivity of the medium ($\epsilon_{\text{average}}$) can be estimated as $\epsilon_{\text{air}} + \epsilon_{SiO_2}$, and doping graphene with TFSA increases $\epsilon_{\text{average}}$ to $\epsilon_{\text{TFSA}} + \epsilon_{SiO_2}$. While the increase in $\epsilon_{\text{average}}$ weakens the Coulomb scattering by charged impurities (and therefore increases μ), charge transfer between TFSA and graphene enhances the charged impurity scattering, leading to overall reduction in μ. Moreover, scattering by thermally excited surface phonons becomes comparable to scattering from charged impurities at room temperature, and the use of an additional dielectric (TFSA) on the other side of the graphene enhances the surface optical phonon scattering (due to increased $\epsilon_{\text{average}}$) [20]. Despite the possible presence of alternative processes contributing to the reduction of mobility in our system, we believe that it is predominantly the combination of these two effects, i.e. charged impurity scattering and thermally excited surface phonon scattering, that causes the overall reduction in μ, consistent with observed reduction in carrier mobility in graphene at higher carrier density [16].

The aforementioned reduction in mobility (scattering time) to 63% of the original value leads to a decrease in the magnitude of the magnetoresistance by a factor of $0.63^2 = 0.4$, which typically scales as MR $\sim (\omega_c\tau)^\alpha$ where ω_c is the cyclotron frequency, τ is the scattering time [21, 22] and α is approximately 2, in qualitative agreement with the curves shown in figure 3(d). At the same time, an increase in n_h manifests itself in metallic-like temperature dependence of R_{graphene} in figure 3(b). R_{graphene} remains unchanged from 300 K down to 50 K, where R_{graphene} starts increasing with decreasing temperature. At temperatures $T \leqslant 50$ K, σ_{graphene} scales as $\sigma_{\text{graphene}} \propto \ln T$, which is indicative of quantum corrections (weak-localization effects) in two dimensions. Doped graphene displays metallic-like behavior as temperature decreases until 20 K, i.e. $R^{\text{graphene}}_{\text{doped}}$ decreases with decreasing temperature, at which point quantum corrections begin to dominate, leading to a slight increase in sheet resistance below 20 K (figure 3(b)).

After discussing the electrical properties of doped and undoped graphene, we now consider the evolution of the Raman spectra by doping. Changes in the Raman spectra of electrically biased graphene and doped graphene sheets with aromatic molecules have been discussed previously, where it has been found that the G and 2D peak positions are sensitive

to the changes in the carrier density [23, 24], allowing the determination of the nature of doping and the corresponding changes in E_F. Figure 4(a) shows the Raman spectra taken at different spots on graphene/SiO_2 and graphene/sapphire samples in the 1200–3000 cm^{-1} range before and after doping. Small D peak intensity and large 2D to G intensity ratio ($I_{2D}/I_G \sim 2.5$) imply that graphene sheets are single layer and are not significantly disordered. After doping with TFSA, unlike with substitutional doping, the intensity of the D peak and hence the density of disorder remain unchanged (figures 4(a)–(c)). Moreover, closer inspection of the G (figure 4(b)) and 2D (figure 4(c)) Raman peak shifts reveals significant changes in peak positions with doping: (1) the G (2D) peak starts at 1588 cm^{-1} (2676 cm^{-1}) and increases up to 1611 $\pm$ 2 cm^{-1} (2692 $\pm$ 3 cm^{-1}), and (2) I_{2D}/I_G decreases from 2.0–2.5 to 0.7–1.0. We note that the TFSA doping brings the G peak position closer to the D′ (disorder activated) peak located at 1620 $\pm$ 2 cm^{-1}. Since the D′ peak is observable when the D peak intensity is much higher than the G and the 2D peak, we do not expect to observe the D′ peak in our system and therefore shifting the G peak up to 1611 $\pm$ 2 cm^{-1} has no effect on our interpretations. These changes in the prominent Raman features of graphene imply that, after doping, the graphene sheets are hole doped and the change in $E_F^{graphene}$ is of the order of 0.5–0.7 eV [23], consistent with our electrical transport measurements, which predict 0.7 eV change in $E_F^{graphene}$ (figure 3).

While TFSA modified graphene shows improved conductivity and superior environmental stability, maintaining graphene's high transparency is important for integrating doped graphene sheets into light emitting devices and solar cells, where harvesting or transmission of light through the graphene layer is critical. Figure 5 shows the transmittance of quartz (black line), graphene/quartz (red line), TFSA/graphene/quartz (blue line), and TFSA/quartz (green line) as a function of wavelength in the 400–800 nm range. Quartz and TFSA/quartz substrates show 95% and 92.8% transmittance respectively, independent of wavelength (λ). After transferring graphene onto quartz substrates, the transmittance of graphene/quartz drops to 92% at 600 nm and the transmittance of graphene, as well as that of TFSA/graphene, becomes a function of λ. Even though TFSA is optically transparent, charge transfer at the TFSA/graphene interface dopes graphene and the increase in carrier density increases (decreases) the overall reflectance (transmittance) by ~3% [25]. Above 800 nm, the transmittance of TFSA/graphene increases monotonically and saturates at 92 $\pm$ 1% at 1500 nm (figure 5(b)), preserving graphene's superior optical properties. More interestingly, while TFSA/graphene possesses high transparency in the near-infrared range with sheet resistance values comparable to those of 150–300 Å thick ITO thin films, ITO starts absorbing light above 1000 nm and its transparency decreases to 25% at 2000 nm. If the electrode can be made both transparent in the near-infrared and conductive, then the light can propagate to the active layers of (a) narrow bandgap based solar cells and (b) novel thermoelectric based cells, which use the Seebeck effect, to be absorbed and converted to electricity. Therefore, unique optical properties of TFSA modified graphene in the visible and near-infrared spectrum with improved conductivity make these films ideal for various applications.

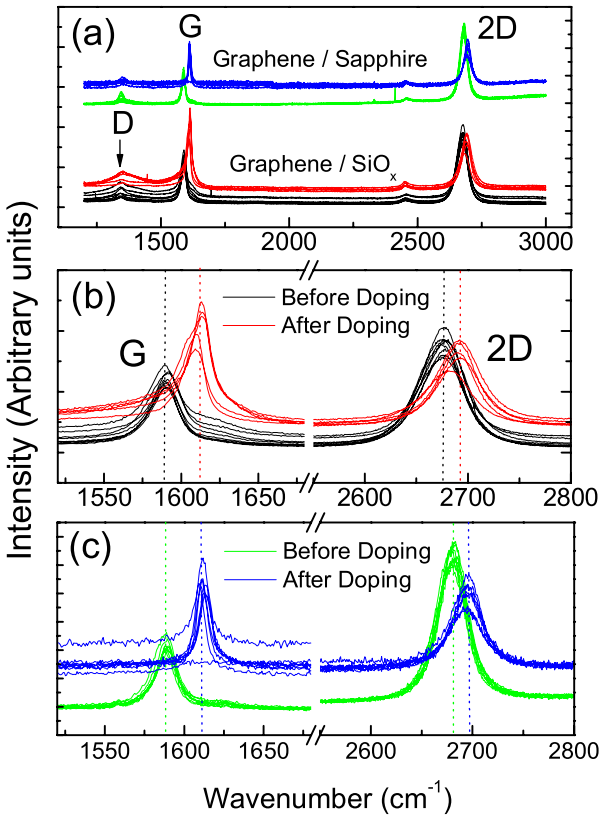

Figure 4. (a) Raman spectrum taken at different spots on the graphene/sapphire (SiO_2) samples before and after the doping. (b) Zoomed in Raman spectra on graphene/SiO_2 before (black line) and after (red line) doping. (c) Zoomed in Raman spectra on graphene/sapphire before (green line) and after (blue line) doping.

4. Conclusion

In conclusion, graphene sheets transferred onto various substrates were p doped with TFSA ($((CF_3SO_2)_2NH)$). Upon modifying graphene with TFSA, the sheet resistance of the samples decreases by 70% of the original value, reaching 129 Ω, and thus is comparable to ITO and FTO values, while samples display superior environmental stability and optical properties. The electrical properties of the doped graphene remain relatively unchanged with time. We attribute the reduction in the sheet resistance to the acceptor nature of the TFSA, increasing the hole carrier density in graphene by 5.2-fold as determined by Hall resistance measurements. Within the Drude formula, the increase in hole carrier density is accompanied by a decrease in the mobility of graphene (to 63% of the original value) but ultimately increases the conductivity of graphene sheets. Raman spectroscopy measurements performed on pristine and doped graphene samples reveal significant shifts in G and 2D peak positions, implying that the E_F of graphene decreases by 0.5–0.7 eV, consistent with the acceptor nature of TFSA and the observed electrical transport

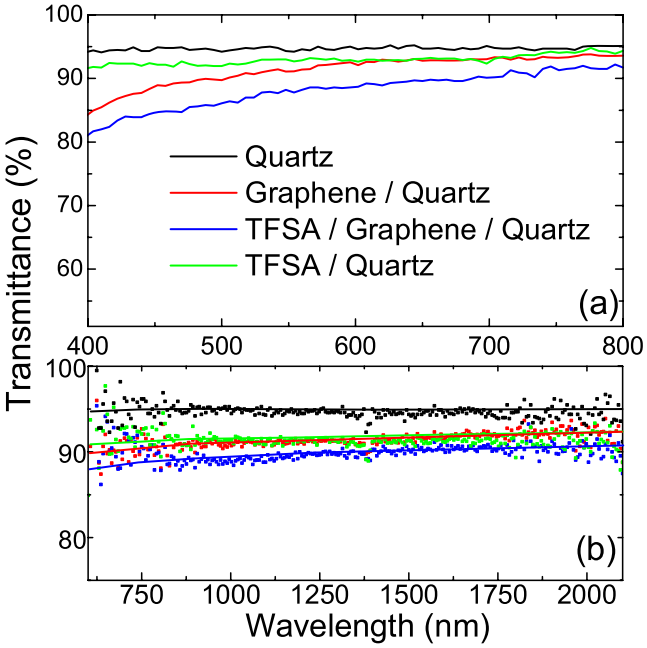

Figure 5. Transmittance versus wavelength taken on pristine quartz (black), graphene/quartz (red), TFSA/graphene/quartz (blue) and TFSA/quartz (green) in the (a) visible and (b) near-infrared spectrum.

properties, from which we have estimated a 0.7 eV decrease in E_F. TFSA doped graphene displays high transparency from 300 to 2500 nm, preserving graphene's optical properties, and is superior to ITO films, where transparency decreases to values of 30–40% in the near-infrared range. The presented results allow us to fabricate environmentally stable graphene sheets with superior electrical–optical properties, giving them a conspicuous advantage for implementation in optoelectronic and solar cell devices and for tuning device characteristics at the graphene/semiconductor interface.

Acknowledgments

This work is supported by the Office of Naval Research (ONR) under contract number 00075094 (BA) and by the National Science Foundation (NSF) under Contract Number 1005301 (AFH).

References

[1] Novoselov K S, Geim A K, Morozov S V, Jiang D, Zhang Y and Dubonos S V 2004 *Science* **306** 666–9
[2] Lin Y M, Jenkins K A, Garcia A V, Small J P, Farmer D B and Avouris P 2009 *Nano Lett.* **9** 422–6
[3] Tongay S, Schumann T and Hebard A F 2009 *Appl. Phys. Lett.* **95** 222103
[4] Tongay S, Schumann T, Miao X, Appleton B R and Hebard A F 2011 *Carbon* **49** 2033–8
Tongay S, Lemaitre M, Schumann T, Berke K, Appleton B R, Gila B and Hebard A F 2011 *Appl. Phys. Lett.* **99** 102102
[5] Li X, Zhu H, Wang K, Cao A, Wei J, Li C, Jia Y, Li Z and Wu D 2010 *Adv. Mater.* **22** 2743–8
[6] Wang X, Zhi L and Mullen K 2008 *Nano Lett.* **8** 323–7
[7] Chen C C, Aykol M, Chang C C, Levi A F J and Cronin S B 2011 *Nano Lett.* **11** 1863–7
[8] Wu J, Becerril H A, Bao Z, Liu Z, Chen Y and Peumans P 2008 *Appl. Phys. Lett.* **92** 263302
[9] Liu H, Liu Y and Zhu D 2011 *J. Mater. Chem.* **21** 3335–45
[10] Farmer D B, Golizadeh-Mojarad R, Perebeinos V, Lin Y-M, Tulevski G S, Tsang J C and Avouris P 2009 *Nano Lett.* **9** 388–92
[11] Schedin F, Geim A K, Morozov S V, Hill E W, Blake B, Katsnelson M I and Novoselov K S 2007 *Nature Mater.* **6** 652–5
[12] Lherbier A, Blase X, Niquet Y-M, Triozon F and Roche S 2008 *Phys. Rev. Lett.* **101** 036808
[13] Wei D, Liu Y, Wang Y, Zhang H, Huang L and Yu G 2009 *Nano Lett.* **9** 1752–8
[14] Kim K K, Reina A, Shi S, Park H, Li L-J, Lee Y H and Kong J 2010 *Nanotechnology* **21** 285205
[15] Li X *et al* 2010 *Nano Lett.* **10** 4328–34
[16] Zhu W, Perebeinos V, Freitag M and Avouris P 2009 *Phys. Rev.* B **80** 235402
[17] Hwang E H, Adam S and Sarma S D 2007 *Phys. Rev. Lett.* **98** 186806
[18] Ando T 2006 *J. Phys. Soc. Japan* **75** 074716
[19] Fratini S and Guinea F 2008 *Phys. Rev.* B **77** 195415
[20] Konar A, Fang T and Jena D 2010 *Phys. Rev.* B **82** 115452
[21] Pippard A B 2009 *Magnetoresistance in Metals* (Cambridge: Cambridge University Press)
[22] Zhi-Min Liao Z-M, Zhou Y-B, Wu H-C, Han B-H and Yu D-P 2011 *Eur. Phys. Lett.* **94** 57004
[23] Das A *et al* 2008 *Nature Nanotechnol.* **3** 210–5
[24] Dong A, Fu D, Fang W, Shi Y, Chen P and Li L-J 2009 *Small* **5** 1422–6
[25] Falkovsky L A 2008 *J. Phys.: Conf. Ser.* **129** 012004